Theory of domain wall motion mediated magnetoelectric effects in a multiferroic composite

V. M. Petrov[1,2] and G. Srinivasan[1,*]

[1]*Physics Department, Oakland University, Rochester, Michigan 48309-4401, USA*

[2]*Institute of Electronic and Information Systems, Novgorod State University, Veliky Novgorod 173003, Russia*

(Received 27 July 2014; published 9 October 2014)

A model is discussed for magnetoelectric (ME) interactions originating from the motion of magnetic domain walls (DWs) in a multiferroic composite of orthoferrites $R\mathrm{FeO_3}$ (RFO) with magnetic stripe domains and a piezoelectric such as lead magnesium niobate-lead titanate (PMN-PT). The DWs in RFO can be set in motion with an ac magnetic field up to a critical speed of 20 km/s, the highest for any magnetic system, leading to the excitation of bulk and shear magnetoacoustic waves. Thus, the ME coupling will arise from flexural deformation associated with DW motion (rather than the Joule magnetostriction mediated coupling under a static or quasistatic condition). A c plane orthoferrite with a single Néel-type DW in the bc plane and an ac magnetic field H along the c axis is assumed. The deflection in the bilayer due to DW motion is obtained when the DW velocity is a linear function H and the resulting induced voltage across PMN-PT is estimated. It is shown that a combination of spatial and time harmonics of the bending deformation leads to (i) a linear ME coefficient defined by $\alpha_E = E/H$ and (ii) a quadratic ME coefficient $\alpha_{\mathrm{EQ}} = E/H^2$. The model is applied to yttrium orthoferrites (YFO) and a PMN-PT bilayer since YFO has one of the highest DW mobility amongst the orthoferrites. The coefficient α_E is dependent on the DW position, and it is maximum when the DW equilibrium position is at the center of the sample. In YFO/PMN-PT the estimated low-frequency $\alpha_E \sim 30$ mV/cm Oe and resonance value is 1.5 V/(cm Oe). Since orthoferrites (and PMN-PT) are transparent in the visible region and have a large Faraday rotation, the DW dynamics and the ME coupling could be studied simultaneously. The theory discussed here is of interest for studies on ME coupling and for applications such as magnetically controlled electro-optic devices.

DOI: 10.1103/PhysRevB.90.144411 PACS number(s): 75.60.−d, 75.80.+q, 77.65.−j, 75.47.Lx

I. INTRODUCTION

A multiferroic is a material that exhibits two or more primary ferroic properties, such as ferromagnetism, ferroelectricity, and ferroelasticity. A composite made of ferromagnetic and ferroelectric phases is a multiferroic that allows for coupling between the electric and magnetic order parameters and is facilitated by mechanical forces [1–6]. The strain mediated magnetoelectric (ME) effect manifests as the polarization of the composite in an applied magnetic field or an induced magnetization/magnetic anisotropy in an electric field. In studies on direct-ME effects, one measures the voltage or polarization induced by applied magnetic fields. For converse-ME effects, the magnetization (or anisotropy field) induced by an electric field is measured. Studies on thick film, thin film heterostructures and nanostructures of ferrites, manganites, or metals/alloys for the ferromagnetic phase and lead zirconate titanate (PZT), barium titanate (BTO), or lead magnesium niobate-lead titanate (PMN-PT) for ferroelectric phases reported a giant low-frequency direct-ME effect [2–4]. A resonant enhancement of ME coupling strength was reported for the composites under bending, longitudinal, or thickness acoustic modes in the samples [3].

Modeling aspects of ME coupling include efforts on single phase materials and in multiferroic composites [7–16]. Past efforts on the theory of strain mediated ME coupling in bulk composites, thin film heterostructures, and nanotubes, nanopillars, and fibers involved Green's function and perturbation theory, the Mori-Tanaka mean field method, thermodynamic approach using Landau-Ginzburg free energy expression, and quasistatic models [8–16]. The influence of sample geometry, interface coupling, material parameters, and demagnetization effects were considered in these models, and estimates of ME coefficients at low frequencies and at resonance were compared with available data [5,9–16].

Here, we report a theory for a novel ME effect that arises due to the motion of magnetic domain walls (DWs) in a multiferroic composite of orthoferrite and ferroelectric. Orthoferrites $R\mathrm{FeO_3}$ (RFO; R = Y, Sm, Er, Ho, etc.) have an orthorhombic structure [17]. The magnetic order is a canted antiferromagnetic with T_c in the range 640–670 K and a weak ferromagnetic moment along the c axis (except for R = Sm) with a room temperature saturation induction $4\pi M$ ranging from 62 G for $\mathrm{NdFeO_3}$ to 143 G for $\mathrm{YbFeO_3}$ [18]. Orthoferrites show a spin-flip transition at low temperatures or at high fields on the order of 75 kOe with the net magnetization aligning along the a axis. Recent studies have reported on a multiferroic character in some orthoferrites [19,20]. The nature of the domains and DWs in RFO films is of particular interest for this report. Thin platelets with the c axis perpendicular to the plane have uniaxial magnetic anisotropy along the c axis and show stripe domains that can be observed in the transmitted light due to the Faraday effect [21]. Due to low magnetization, the stripe domains in RFO are large in size compared to similar domains in yttrium iron garnet and spinel or hexagonal ferrites [21–24]. The DWs in the ac plane are Bloch walls and those in the ab or bc planes are Néel walls with ∼0.1–1 μm in width. The DWs have excellent mobility [18]. Under the influence of an external ac magnetic field H, a DW can be set in motion up to a maximum speed of 20 km/s, which is the highest for any magnetic system [24–27]. This speed is a factor of three to five higher than for transverse and longitudinal acoustic waves in orthoferrites. The subsonic or supersonic motion of

*srinivas@oakland.edu

Bloch or Néel walls leads to the excitation of bulk and surface magnetoacoustic waves [27]. High power lasers also were used to excite such waves in YFO [28].

Kuzmenko *et al.* [27] recently developed a theory for the excitation of magnetoacoustic waves due to DW motion in *R*FO and also measured their amplitude. For modeling, they considered a Néel type wall in *bc* (or *YZ*) plane of YFO and DW motion along the *a* (or *X*) axis due to an ac field along the *c* axis. Equations of motion for the net magnetization along *Z* direction were solved, taking into consideration exchange interactions, magnetic anisotropy, magnetoelastic constants, and strain tensor for YFO. The theory predicted two types of waves, bulk (Rayleigh-Lamb) waves with flexural amplitude u_z and surface waves with amplitude u_x. The surface wave amplitude is smaller than u_z. Our model discussed here predicts a strong ME effect associated with these flexural magnetoacoustic waves in a composite with a ferroelectric.

A bilayer of *R*FO and ferroelectric $(1-x)$ $Pb(Mg_{1/3}Nb_{2/3})O_3$ $-$ x $PbTiO_3$ [PMN-PT] is considered. Lead magnesium niobate-lead titanate is a relaxor ferroelectric with a diffused phase transition, frequency dependent dielectric maxima, and nonlinear dielectric response for bias voltage [29,30]. The crystal structure and the ferroelectric nature are critically dependent on x [30]. Also, PMN-PT shows a morphotropic phase transition around 33% Ti. Much interest is focused on compositions close to $x \sim 0.33$ because of their large piezoelectric constants [29]. The (001) PMN-PT compositions with $x = 0.30$–0.34 have a high piezoelectric coefficient $d_{33} \sim 1500$–2500 pm/V for strong ME coupling [30]. Single crystal PMN-PT of nominal thickness (~0.5 mm) is transparent to visible light and is suitable for simultaneous ME measurements and optical observation of DWs in the *R*FO/PMN-PT composites [31,32].

Here we report on a model for DW motion mediated ME interactions in *R*FO/ferroelectric bilayers. The direct ME effect, i.e., the electric field or voltage induced due to the motion of a single DW in an applied ac magnetic field, is considered. A bilayer of a ferroelectric and a *c* plane orthoferrite in a two-domain state and a single Néel-type DW in the *bc* plane is assumed. An ac magnetic field along the *c* axis will lead to the motion of the DW, and a shear force associated with the moving wall gives rise to a flexural deformation. We solve the equation of motion for the case when the DW velocity is a linear function of the ac field strength. The deflection in the orthoferrite-ferroelectric bilayer is obtained, and the induced voltage across the ferroelectric layer due to piezoelectric effect is estimated. The theory predicts a strong ME coupling at low frequencies and a resonance enhancement at bending mode frequencies for the bilayer. It is shown that, for direct-ME effect, the combination of spatial and time harmonics of the bending mode leads to (i) a linear ME coefficient defined by $\alpha_E = E/H$ and (ii) a quadratic ME coefficient $\alpha_{EQ} = E/H^2$. The coefficient α_E is dependent on the DW position, and it is maximum when the DW equilibrium position is at the center of the sample. The model is then applied to the specific case of YFO/PMN-PT since YFO has one of the highest DW mobility among the orthoferrites and PMN-PT has a very high piezoelectric coupling coefficient. In YFO/PMN-PT, the estimated low-frequency $\alpha_E \sim 30$ mV/cm Oe and the resonance value of 1.5 V/cm Oe compare favorably with ME voltage coefficients for Joule magnetostriction mediated ME coupling in ferromagnetic-ferroelectric composites. In the sections that follow, the theory and the application to YFO/PMN-PT are discussed.

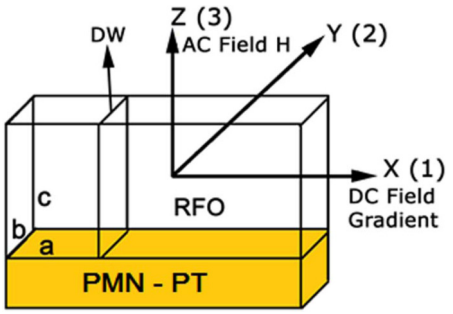

FIG. 1. (Color online) Diagram showing a bilayer of *c* plane orthoferrite $RFeO_3$ and ferroelectric PMN-PT. A dc magnetic field gradient along the *X* direction stabilizes a single magnetic DW in the *bc* plane. The DW can be set in motion along the *X* direction by applying an ac magnetic field *H* along the *Z* direction.

II. THEORY

We consider a bilayer of *c* plane platelet of *R*FO and (001) PMN-PT as shown in Fig. 1. A coordinate system with the origin at the center of the sample, *a* axis of *R*FO along the *X* (1) direction and *b* axis along the *Y* (2) axis is assumed. The *c* plane platelet of orthoferrite is assumed to be in a two-domain state (with the aid of an in-plane dc magnetic field gradient along the *X* direction) with a Néel-type DW in the *bc* plane. An ac magnetic field is assumed along the *Z* (3) axis (perpendicular to the sample plane). The theory that follows has the following steps. (i) We consider the single DW motion and obtain the amplitude vs driving field and frequency characteristics. (ii) The DW displacement is then used to estimate the transverse (shear) force acting on the sample. (iii) The shear force acting across the region of DW that produces a flexural deformation is represented by two δ functions. (iv) We solve a relevant differential equation of motion to obtain the deflection of the sample due to the shear force. (v) Then the longitudinal (along *X* axis) deformation of the ferroelectric layer is estimated from the deflection. (vi) The electric field generated across the ferroelectric layer due to piezoelectric effect is calculated. (vii) The ME coefficient due to DW motion is thus obtained.

The DW motion under the influence of the ac magnetic field is described by the equation [33–35]

$$m\ddot{x}_W + \beta\dot{x}_W + \alpha x_W = 2MH\exp(i\omega t) \qquad (1)$$

where H is the amplitude of the ac drive field of frequency ω, M is the net magnetization of orthoferrite layer, x_w is the displacement of the wall from equilibrium, β is a viscous damping parameter, α is the restoring pressure per unit wall displacement, and m is an effective mass characterizing the inertial properties of the wall. Within a frequency range well below DW resonance $\omega_r = \sqrt{\alpha/m}$ (typically 100 MHz), we can neglect $(\omega/\omega_r)^2$ compared to unity, and consequently the inertial term in Eq. (1) can be omitted. For this case, the approximate solution for wall displacement is given

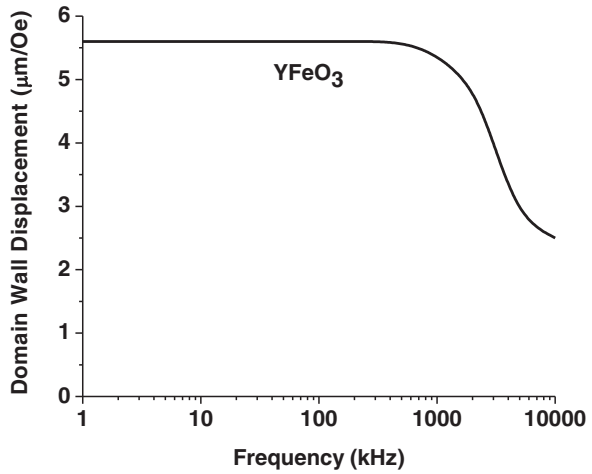

FIG. 2. Measured frequency dependence of DW displacement in yttrium orthoferrites at room temperature (from Ref. [36]).

by Ref. [34]

$$|x_W| = x_0\left[1+\left(\frac{\omega}{\omega_c}\right)^2\right]^{-1/2}, \tag{2}$$

where $x_0 = 2MH/\alpha$ is the low-frequency limit of displacement and $\omega_c = \alpha/\beta$ is the relaxation frequency. Figure 2 shows the measured frequency dependence of DW displacement in YFO [36]. One could then use Eq. (2) and the data in Fig. 2 to obtain the amplitude of DW displacement and the resulting transverse force for estimation of the strength of ME coupling.

A DW is known to produce a shear deformation due to magnetoelastic coupling [37]. The shear deformation is due to the Wiedemann effect that originates from orthogonal magnetization or magnetic fields [38]. A shear deformation S_5 is expected under DW motion since the magnetization components M_1 and M_3 are nonzero. The DW motion thus results in a transverse force confined to the moving DW in the RFO layer. For the Néel type DW in the bc (YZ) plane, this force per unit width equals ${}^{m}T_5{}^{m}t$ with ${}^{m}T_5$ denoting the stress component in the orthoferrite layer. The thickness of the sample is assumed to be small compared to other dimensions and its width small compared to its length. In that case, we need to consider only one component of strain and stress. The equation of bending motion for the middle plane of bilayer has the form

$$\nabla^2\nabla^2 w + \frac{\rho t}{D}\frac{\partial^2 w}{\partial \tau^2} = \frac{1}{D}f(x,\tau), \tag{3}$$

where $\nabla^2\nabla^2$ is the biharmonic operator, w is the deflection (displacement in Z direction), t and ρ are the thickness and average density of the sample, respectively, D is the cylindrical stiffness, $f(x,\tau)$ is the load intensity due to DW motion, and τ is the time. For a bilayer, total thickness $t = {}^{p}t + {}^{m}t$ and average density $\rho = ({}^{p}\rho\,{}^{p}t + {}^{m}\rho{}^{m}t)/t$, where ${}^{p}\rho$, ${}^{m}\rho$, ${}^{p}t$, and ${}^{m}t$ are densities and thicknesses of ferroelectric and magnetic layers, respectively. The load intensity is defined as the magnetostrictive force per unit width of the sample. In turn, the magnetostrictive force can be found from the magnetoelastic energy density

$$\Phi_{\mathrm{ME}} = (\mu_1 S_1 + \mu_3 S_3)\sin^2\theta + \mu_5 S_5 \sin(2\theta), \tag{4}$$

where μ_i and θ are the magnetoelastic constants and angle between the c axis and ferromagnetic moment [39], and S_i are the strain components. For periodic DW motion, the load intensity has a point of application of $x_{\mathrm{DW}} = x_1 + x_W\cos(\omega\tau)$ with x_1, x_W, and ω denoting the distance of equilibrium position of DW from the center of the sample, peak displacement of the DW, and angular frequency of the driving magnetic field, respectively. Thus, one-dimensional (1D) approximation of Eq. (3) takes on the form

$$\frac{\partial^4 w}{\partial x^4} + \frac{\rho t}{D}\frac{\partial^2 w}{\partial \tau^2} = \frac{1}{2D}\mu_5{}^{m}t[\delta(x - x_1 - x_W\cos\omega\tau) - \delta(x - x_1 - \Delta/2 - x_W\cos\omega\tau)], \tag{5}$$

where Δ is the DW width and the introduction of δ functions is enabled due to small DW displacement compared to the sample length. Note that the force associated with DW motion is modeled by two δ functions since the transverse force vanishes at the wall borders and wall center and has two maxima with a distance of $\Delta/2$ between the two.

The δ functions can be expanded as a Fourier series in eigenfunctions of corresponding homogeneous differential equations, i.e., Eq. (5) with the right part zero. For a freely supported sample, one gets the series for

$$\delta(x - x_1 - x_W\cos\omega\tau) - \delta(x - x_1 - \Delta/2 - x_W\cos\omega\tau) = \frac{A_0}{2} + \sum_{n=1}^{\infty} A_n\cos\frac{n\pi x}{L} + \sum_{n=1}^{\infty} B_n\sin\frac{n\pi x}{L}, \tag{6}$$

where L is the sample length, and A_n and B_n are Fourier coefficients that, in turn, can be expanded as power series in $\cos\omega\tau$. The final expression for deflection can be obtained as a double series in spatial and time harmonics by substituting the expansion of the δ function into Eq. (5). For finding the ME voltage induced due to an applied ac magnetic field, the stress component in the piezoelectric layer should be expressed in terms of deflection as ${}^{p}T_1 = -{}^{p}Y(z\frac{\partial^2 w}{\partial x^2} + {}^{p}d_{31}{}^{p}E_3)$, where z is measured from the middle plane of the sample. The middle plane is defined as the plane for which the displacement is only along Z. In this expression, ${}^{p}Y$, ${}^{p}d_{31}$, and ${}^{p}E_3$ are Young's modulus, piezoelectric coefficient, and electric field generated across the piezoelectric layer, respectively. Assuming an open circuit condition, the electric field in the piezoelectric layer ${}^{p}E_3$ can be found from the equation

$${}^{p}E_3 = -\frac{{}^{p}d_{31}}{L\,{}^{p}\varepsilon_{33}}\int_{-L/2}^{L/2} {}^{p}T_1 dx, \tag{7}$$

where ${}^{p}\varepsilon_{33}$ is permittivity. Thus, the average induced electric field E across the piezoelectric layer is given by

$$E = \frac{1}{{}^{p}t}\int_{z_0-{}^{p}t}^{z_0} {}^{p}E_3 dz, \tag{8}$$

with z_0 denoting the distance of the middle plane from the orthoferrite/piezoelectric interface. It is clear from Eqs. (5) and (6) that E is a function of integral multiples of frequency ω. One therefore needs to consider harmonics in space and time in order to estimate the ME coefficients. We use the designation

$n = 1, 2, 3 \ldots$ for spatial harmonics and $m = 1,2 \ldots$ for time harmonics. Since we consider a freely supported bilayer, the coefficient $B_n = 0$ in the expansion in Eq. (6). Specific harmonics of bending modes in space and time are discussed next.

(i) First spatial harmonic and first time harmonic ($n = m = 1$): To illustrate the use of Eqs. (5)–(8) for estimating the ME coupling coefficient, we consider the DW displaced by distance x_1 from the sample center. The ME coefficient for this case must be estimated for the term $A_1 \cos \frac{\pi x}{L}$ in the Fourier series for the δ functions with

$$A_1 = \frac{\pi^2 x_W \Delta}{48L^6}\left[\left(24L^2 - 12\pi^2 x_1^2 - 6\pi^2 x_1 \Delta - \pi^2 \Delta^2\right)\cos\omega\tau - 3\pi^2 x_W (4x_1 + \Delta)\cos^2\omega\tau - 4\pi^2 x_W^2 \cos^3\omega\tau\right]. \tag{9}$$

The above equation contains terms with $\omega\tau$, $2\omega\tau$, and $3\omega\tau$ ($m = 1$, 2, and 3, respectively). We define the fundamental mode as $n = m = 1$ with the coefficient $A_{1,1} = (1 - \frac{\pi^2 x_1^2}{2L^2})\frac{\pi^2}{L^3}\Delta x_W \cos\ \omega\tau$. For this case, solutions of Eq. (5) can be written as $w(x, \tau) = u(x)\cos\omega\tau$. The equation for $u(x)$ has the form

$$\frac{d^4u}{dx^4} - k^4 u = \frac{1}{2D}\mu_5{}^m t\left(1 - \frac{\pi^2 x_1^2}{2L^2}\right)\frac{\pi^2}{L^3}\Delta x_W \cos\ \frac{\pi x}{L}, \tag{10}$$

where $k^4 = \omega^2 \frac{\rho t}{D}$. The particular solution of Eq. (10), which satisfies the end conditions for freely supported ends of the sample is as follows:

$$u(x) = \frac{{}^p d_{31} E\, {}^pY\, {}^p t({}^p t - 2z_0)\left[\cos(kx)\cosh\left(\frac{kL}{2}\right) - 4\cosh(kx)\cos\left(\frac{kL}{2}\right)\right]}{4k^2 D\cos\left(\frac{kL}{2}\right)\cosh\left(\frac{kL}{2}\right)} + \frac{\mu_5 \Delta\pi^2 x_W{}^m t L\cos\left(\frac{\pi x}{L}\right)}{2D(\pi^4 - k^4L^4)}\left(1 - \frac{\pi^2 x_1^2}{2L^2}\right). \tag{11}$$

This expression could be used for finding the stress component ${}^p t_1$, which enables calculating the electric field E and assuming ${}^p K_{31}$, the electromechanical coupling factor, satisfies the condition ${}^p K_{31}^2 \ll 1$. The electric field E is determined from

$$E = H\frac{{}^p d_{31}\, {}^pY\, {}^mY \mu_5 \Delta\pi^3 x_{W1}\left(2L^2 - \pi^2 x_1^2\right){}^m t^2 t}{4DL^3(\pi^4 - k^4L^4)({}^pY\, {}^p t + {}^mY\, {}^m t)\, {}^p\varepsilon_{33}}, \tag{12}$$

where $x_{W1} = x_W/H$ is the DW displacement per unit drive field. Since E is a linear function of H, one may define the ME coefficient for this specific case as $\alpha_{E\,(1,1)} = E/H$. In the low-frequency limit, $\alpha_{E\,(1,1)} = E/H$ is given by

$$a_{E(1,1)} = E/H; \quad \mathrm{E} = H\frac{{}^p d_{31}\, {}^pY\, {}^mY \mu_5 \Delta x_{W1}\left(2L^2 - \pi^2 x_1^2\right){}^m t^2 t}{4DL^3\pi({}^pY\, {}^p t + {}^mY\, {}^m t)\, {}^p\varepsilon_{33}}. \tag{13}$$

(ii) First spatial harmonic and second time harmonic ($n = 1$, $m = 2$): Next we consider the term with $2\omega\tau$ in Eq. (9) with the coefficient $A_{1,2} = -\frac{\pi^2}{4L^3}x_W^2 \cos\ 2\omega\tau$. For this case, the solution of Eq. (5) can be written as $w(x, \tau) = u(x)\cos 2\omega t$. Substituting $A_1 \cos\frac{\pi x}{L}$ in place of the δ function into Eq. (5) leads to the following equation for $u(x)$:

$$\frac{d^4u}{dx^4} - 4k^4 u = \frac{1}{8D}\mu_5 \Delta\frac{\pi^4 x_W^2{}^m t x_1}{L^5}\cos\ \frac{\pi x}{L}. \tag{14}$$

The particular solution of Eq. (14), which satisfies the end conditions for freely supported ends of the sample is as follows:

$$u(x) = \frac{{}^p d_{31} E\, {}^pY\, {}^p t({}^p t - 2z_0)\left[\cos(\sqrt{2}kx)\cosh\left(\frac{kL}{\sqrt{2}}\right) - 4\cosh(\sqrt{2}kx)\cos\left(\frac{kL}{\sqrt{2}}\right)\right]}{4k^2 D\cos\left(\frac{kL}{\sqrt{2}}\right)\cosh\left(\frac{kL}{\sqrt{2}}\right)} - \frac{\mu_5{}^m t\pi^4 x_W^2 x_1 \Delta L\cos\left(\frac{\pi x}{L}\right)}{8DL(\pi^4 - 4k^4L^4)}. \tag{15}$$

Since $u(x)$ is a function x_W^2 in Eq. (15), the deflection and consequently induced electric field are quadratic functions of the applied ac magnetic field. This suggests introducing the ME coefficient $\alpha_{\mathrm{EQ}\,(1,2)}$ for the case of quadratic ME coupling as follows:

$$\alpha_{\mathrm{EQ}\,(1,2)} = \frac{E}{H^2} = \frac{1}{{}^p t H^2}\int_{z_0 - {}^p t}^{z_0} {}^p E_3 dz, \quad \text{and} \tag{16}$$

$$\alpha_{\mathrm{EQ}\,(1,2)} = \frac{{}^p d_{31}\, {}^pY\, {}^mY \mu_5 \Delta\pi^5 x_{W1}^2 x_1{}^m t^2 t}{8DL^3(\pi^4 - 4k^4L^4)({}^pY\, {}^p t + {}^m Y\, {}^m t)\, {}^p\varepsilon_{33}}. \tag{17}$$

(ii) Second spatial harmonic: For the second spatial harmonic, the deflection of the sample is an odd function of x. Taking this into consideration, induced voltage vanishes according to Eq. (7) since it is calculated as the integral of the odd function over the full period. Thus, ME coefficients $\alpha_{E(2,1)}$ and $\alpha_{E(2,2)}$ become zero.

(iii) Third spatial harmonic: The third spatial harmonic will give rise to an ME response as discussed below. For this case, the term $A_3 \cos\frac{3\pi x}{L}$ in the series for the δ function, and assuming the solution of Eq. (5) to be $w(x, t) = u(x)\cos\omega t$, leads to the following expression for $u(x)$:

$$u(x) = \frac{{}^p d_{31} E\, {}^pY\, {}^p t({}^p t - 2z_0)\left[\cos(kx)\cosh\left(\frac{kL}{2}\right) - 4\cosh(kx)\cos\left(\frac{kL}{2}\right)\right]}{4k^2 D\cos\left(\frac{kL}{2}\right)\cosh\left(\frac{kL}{2}\right)} + \frac{9\mu_5 \Delta\pi^{2m} t x_W\left(2L^2 - 9\pi^2 x_1^2\right)\cos\left(\frac{3\pi x}{L}\right)}{8D(81\pi^4 - k^4L^4)}. \tag{18}$$

This expression enables finding the stress component ${}^{p}t_1$, and then the ME voltage coefficient for the first time harmonic is given by

$$\alpha_{E(3,1)} = E/H = \frac{27\,{}^{p}d_{31}\,{}^{p}Y\,{}^{m}Y\,\mu_5\Delta\pi^3 x_{W1}\,{}^{m}t^2 t\left(9\pi^2 x_1^2 - 2L^2\right)}{8DL^3(81\pi^4 - k^4L^4)({}^{p}Y\,{}^{p}t + {}^{m}Y\,{}^{m}t)\,{}^{p}\varepsilon_{33}}. \tag{19}$$

The expression for $\alpha_{\mathrm{EQ}\,(3,2)}$ for the third spatial and second time harmonic is obtained using a procedure similar to the previous case for $\alpha_{\mathrm{EQ}\,(1,2)}$

$$\alpha_{\mathrm{EQ}\,(3,2)} = \frac{343\,{}^{p}d_{31}\,{}^{p}Y\,{}^{m}Y\,\mu_5\Delta\pi^5 x_{W1}^2 x_1\,{}^{m}t^2 t}{16DL^3(81\pi^4 - 4k^4L^4)({}^{p}Y\,{}^{p}t + {}^{m}Y\,{}^{m}t)\,{}^{p}\varepsilon_{33}}. \tag{20}$$

It is clear from the expressions for α_E that the ME coefficients are directly proportional to the product ${}^{m}t^2\,t$. One could achieve a strong ME response by increasing the thickness of the orthoferrites. Application of the theory to specific orthoferrite-ferroelectric bilayers is considered next.

III. APPLICATION TO YFO/PMN-PT AND DISCUSSION

Next, we apply the theory to a representative bilayer, i.e., $YFeO_3$/PMN-PT. Since thick films of both YFO and PMN-PT are transparent in the visible region, simultaneous measurements on DW motion and ME effect are possible in such systems. Another advantage is the very high mobility for DW in YFO that will lead to a strong ME coupling in the bilayer. The theory in Sec. II is valid when the DW displacement and, therefore, the velocity is a linear function of the ac magnetic field amplitude H. Measurements of the velocity of Néel-type DWs by optical techniques were reported in a series of *R*FO samples [21,36,40,41]. For YFO, DW speed v at 300 K increased linearly with $H$for $H < 1$ kOe, followed by a nonlinear dependence up to the limiting speed of $c \sim 20$ km/s, which is much higher than the speed of transverse sound waves $s_t = 4$ km/s [40]. In the data on v vs H, there are regions close to s_t and multiples of s_t over which v remained constant or showed nonlinear dependence on H [40]. We, however, restrict our discussion here to the linear v vs H region.

A bilayer of lateral dimensions 9.2 × 1 mm and YFO of thickness 100 μm and PMN-PT of thickness of 50 μm is assumed. The above sample dimensions were chosen in order to achieve a desired resonance frequency of around ~3 kHz for the acoustic modes. The resonance frequencies for a freely supported sample are known to be determined by the equation $\sin(kL) = 0$ where the wave number k is defined by the expression $k^4 = \frac{\omega^2\rho t}{D}$ with ρ and D denoting the average density and cylindrical stiffness of the sample. D is known to be dependent on layer thicknesses and sample length. Thus, the resonance frequencies are closely related to the sample geometry. The selection of the sample length and layer thicknesses is stipulated by appropriate values of resonance frequencies. In turn, the resonance frequencies are taken so that they are much lower compared to the DW relaxation frequency to avoid an additional decrease in DW displacement in the applied drive field (see Fig. 2).

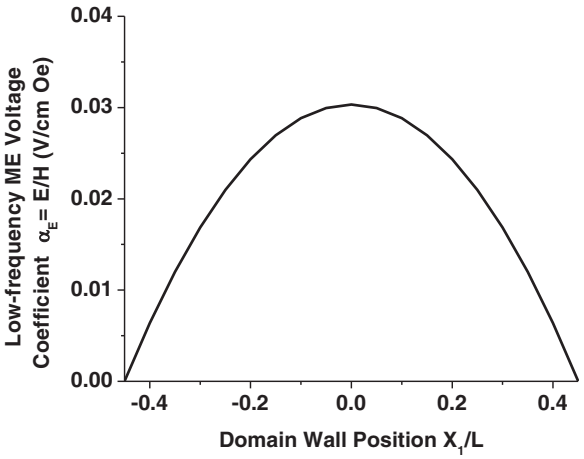

FIG. 3. Variation of low-frequency ME voltage coefficient with the equilibrium DW position relative to sample center for $YFeO_3$/PMN-PT bilayer.

The following material parameters were assumed for YFO and PMN-PT: ${}^{m}Y = 1.9 \cdot 10^{11}$ N/m^2, ${}^{p}Y = 0.77 \cdot 10^{11}$ N/m^2, ${}^{m}\rho = 5.5 \cdot 10^3$ kg/m^3, ${}^{p}\rho = 7.7 \cdot 10^3$ kg/m^3, ${}^{p}\varepsilon_{33}\varepsilon_0 = 5000$, ${}^{p}d_{31} = -600 \cdot 10^{-12}$ m/V, $\mu_5 = 1.2 \cdot 10^6$ J/m^3, and $\Delta = 0.1$ μm [39,42]. Resonance losses are accounted by using a complex frequency $\omega + i\omega'$ with $\omega'/\omega = 10^{-2}$. Consider first the low-frequency linear ME coefficient given by Eq. (13). Figure 3 shows $\alpha_{E(1,1)}$ vs the position of the DW for the low-frequency region. The ME coupling is maximum with a value of ~30 mV/cm Oe when the DW is at the center of the sample (at $x_1 = 0$). A decrease in α_E is evident as the DW equilibrium position is moved away from the center and it vanishes for $x_1 = \pm L/2$. A significant enhancement in the α_E value is expected when the frequency of the applied field H is at the bending mode for the bilayer, as discussed next.

The linear ME coefficient $\alpha_E = E/H$ for the first time harmonic of the first and third spatial harmonics, $\alpha_{E\,(1,1)}$ and $\alpha_{E(3,1)}$, respectively, are shown as a function of frequency f in Fig. 4. The resonance value of $\alpha_{E1,1}$ is very much dependent on the DW position [Eqs. (16) and (19)], similar to the case of low-frequency ME coupling in Fig. 3, and is ~0.4 V/cm Oe for $x_1 = 0.4\,L$ at 3.45 kHz. The estimated frequency f dependence of the quadratic ME coefficient $\alpha_{\mathrm{EQ}} = E/H^2$ for the first and third spatial harmonics are shown in Fig. 5. The results indicate a resonance enhancement in ME coupling strength when $2f = f_r$, the bending mode frequency for the bilayer. The quadratic ME coupling strength is linearly dependent on the equilibrium position of the DW [Eqs. (17) and (20)]. Figures 4 and 5 reveal that the output voltage induced by the magnetic field $H = 1$ Oe for the second time harmonic is much smaller than for the first time harmonic.

The model developed here deals with ME coupling in *R*FO/ferroelectric composites arising from magnetoelastic excitations associated with DW motion (rather than Joule magnetostriction mediated coupling under the quasistatic condition in ferromagnetic-ferroelectric composites). Since the DW motion is a magnetization reversal process (at a field much lower than ~75 kOe required for spin-flip), it gives rise to bulk magnetoacoustic waves. Our model predicts that this flexural deformation when coupled with the piezoelectric phase will

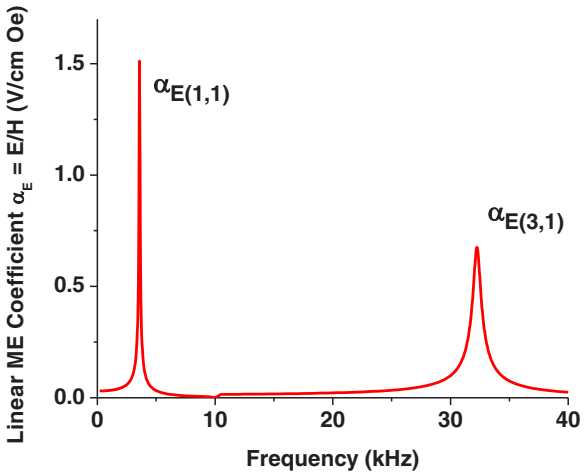

FIG. 4. (Color online) Frequency dependence of the linear ME voltage coefficient in a bilayer of $YFeO_3$ and PMN-PT for the DW located at the center of the sample. Results are for the first time harmonic of the first and third spatial harmonics, $\alpha_{E(1,1)}$ and $\alpha_{E(3,1)}$, respectively.

result in a strong ME coupling. Variation of the linear ME voltage coefficient with the equilibrium DW position relative to the sample center is described by Eq. (13) and is shown in Fig. 3. The maximum value of $\alpha_{E(1,1)}$ is obtained at the DW position at the sample center. The linear ME effect vanishes for the DW position at the sample ends. The quadratic ME coupling strength is linearly dependent on the equilibrium position of the DW [Eqs. (17) and (20)]. It vanishes for the DW position at the sample center. The presence of multiple DWs will result in a partial cancellation of contributions to output voltage due to a difference in motion direction for DWs because of different magnetization directions. Thus, the ME coupling for multiple DWs is expected to be weaker compared to a single DW. It should be noted that the generation of multiple DWs by a dc magnetic field gradient is rather complicated. An appropriate dc field gradient produces the

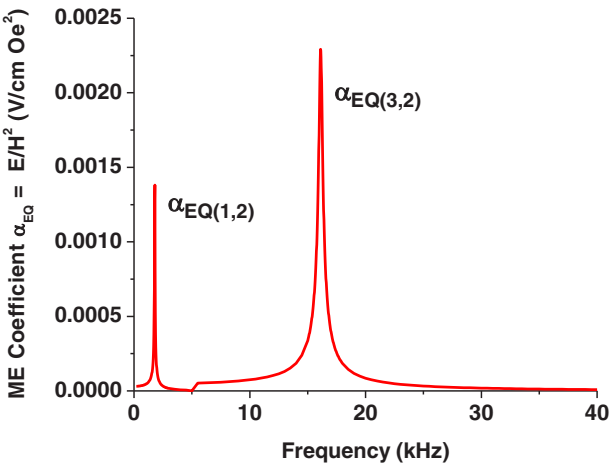

FIG. 5. (Color online) Frequency dependence of the quadratic ME coefficient α_{EQ} in a bilayer of $YFeO_3$ and PMN-PT for the DW located at distance $L/4$ from the center of the sample. Results are for the first and third spatial harmonics.

single DW which is positioned at the point with zero dc magnetic field. It is important to compare theoretical estimates of α_E with measured values of α_E for strain mediated ME coupling in ferromagnetic-ferroelectric composites. The low-frequency α_E in Fig. 3 for YFO/PMN-PT compares favorably with bulk ferrite-ferroelectric composites [3]. The peak values of α_E in Fig. 4 are also comparable to ME voltage coefficients at bending modes or longitudinal acoustic modes in several composites of ferromagnets and PZT or PMN-PT [3].

The theory is valid only when the speed of DW motion v is a linear function of H. Under high mobility and supersonic speeds, v vs H is nonlinear and shows regions of constant v due to damping attributed to the Cherenkov emission of phonons [37]. The DW shows a transition from a straight 1D wall to a distorted two-dimensional (2D) wall for supersonic speeds. It is therefore necessary to formulate a theory of ME coupling under a rich variety of phenomena associated with the DW motion, such as nonlinearity under high mobility and high H, instability of rectilinear DW motion, transition to a 2D wall and the formation of kinks on a DW under supersonic speed, and DW dynamics at the critical velocity c [22,24,25–27,40,41].

IV. CONCLUSIONS

A theory is developed for the nature of magnetoelectric coupling due to magnetic DW motion in a bilayer of orthoferrite and ferroelectric. Orthoferrites that are canted antiferromagnets show a weak ferromagnetic moment along the c axis and a stripe domain structure at room temperature. A single Néel-type DW in the bc plane can be stabilized with a static magnetic field gradient along the a axis. The DW can be set in motion with an ac magnetic field H along the c axis. Domain wall speeds v could reach a maximum of 20 km/s in orthoferrites and generate bulk flexural and surface shear magnetoacoustic waves. Such excitations in a bilayer of orthoferrite and a ferroelectric will result in a bending motion and an induced electric field E across the ferroelectric layer thickness. The model developed here considers ME coupling due to bending deformation for linear v vs H. It is shown that spatial and time harmonics of the bending mode lead to (i) a linear ME coefficient defined by $\alpha_E = E/H$ for first time harmonic modes and (ii) a quadratic ME coefficient $\alpha_{EQ} = E/H^2$ for the second time harmonic modes. The coefficient α_E shows a peak at the bending resonance frequency and is found to be dependent on the DW position with the maximum value expected when the DW equilibrium position is at the center of the sample. In YFO/PMN-PT, the maximum value of α_E is on the order of 30 mV/cm Oe at low-frequency 1.5 V/cm Oe at the first spatial harmonic. The quadratic ME coefficient α_{EQ} is predicted to be rather weak compared to the line ME coefficient.

ACKNOWLEDGMENTS

The research at Oakland University was supported by a grant from the National Science Foundation (Grant No. ECCS-1307714). The work at Novgorod State University was supported by RFBR research Project No. 14-42-06005 and by the Ministry of Education and Science of the Russian Federation in the framework of the Government Order for Higher Schools.

[1] N. A. Spaldin and M. Fiebig, Science **309**, 391 (2005).
[2] J. Zhai, Z. Xing, S. Dong, J. Li and D. Viehland, J. Am. Ceram. Soc. **91**, 351 (2008).
[3] C.-W. Nan, M. I. Bichurin, S. Dong, D. Viehland, and G. Srinivasan, J. Appl. Phys. **103**, 031101 (2008).
[4] C. A. F. Vaz, J. Hoffman, C. H. Ahn, and R. Ramesh, Adv. Mater. **22**, 2900 (2010).
[5] J. Ma, J. Hu, Z. Li, and C. W. Nan, Advan. Mater. **23**, 1062 (2011).
[6] L. W. Martin and R. Ramesh, Acta Materialia **60**, 2449 (2012).
[7] G. T. Rado and J. M. Ferrari, Phys. Rev. B **15**, 290 (1977).
[8] E. Bousquet and N. Spaldin, Phys. Rev. Lett. **107**, 197603 (2011).
[9] C.-W. Nan, Phys. Rev. B **50**, 6082 (1994).
[10] M. I. Bichurin, I. A. Kornev, V. M. Petrov, A. S. Tatarenko, Y. V. Kiliba, and G. Srinivasan, Phys. Rev. B **64**, 094409 (2001).
[11] M. I. Bichurin, V. M. Petrov, and G. Srinivasan, Phys. Rev. B **68**, 054402 (2003).
[12] G. Srinivasan, C. P. De Vreugd, V. M. Laletin, N. Paddubnaya, M. I. Bichurin, V. M. Petrov, and D. A. Filippov, Phys. Rev. B **71**, 184423 (2005).
[13] M. I. Bichurin, V. M. Petrov, O. V. Ryabkov, S. V. Averkin, and G. Srinivasan, Phys. Rev. B **72**, 060408(R) 2005.
[14] V. M. Petrov, G. Srinivasan, M. I. Bichurin, and A. Gupta, Phys. Rev. B **75**, 224407 (2007).
[15] C.-M. Chang and G. P. Carman, Phys. Rev. B **76**, 134116 (2007).
[16] X. Wang and E. Pan, Phys. Rev. B **76**, 214107 (2007).
[17] E. A. Giess, Science **208**, 938 (1980).
[18] R. L. White, J. Appl. Phys. **40**, 1061 (1969).
[19] J. H. Lee, Y. K. Jeong, J. H. Park, M. A. Oak, H. M. Jang, J. Y. Son, and J. F. Scott, Phys. Rev. Lett. **107**, 117201 (2011).
[20] P. Mandal, V. S. Bhadram, Y. Sundarayya, C. Narayana, A. Sundaresan, and C. N. R. Rao, Phys. Rev. Lett. **107**, 137202 (2011).
[21] F. C. Rossol, J. Appl. Phys. **40**, 1082 (1969).
[22] F. C. Rossol, Phys. Rev. Lett. **24**, 1021 (1970).
[23] L. T. Tsymbal, G. N. Kakazei, and Ya. B. Bazaliy, Phys. Rev. B **79**, 092414 (2009).
[24] R. C. Sherwood, J. P. Remeika, and J. Williams, J. Appl. Phys. **30**, 217 (1959).
[25] A. P. Kuzmenko, E. A. Zhukov, and M. B. Dobromyslov, J. Magn. Magn. Mater. **302**, 436 (2006).
[26] A. P. Kuzmenko, V. K. Bulgakov, A. V. Kaminsky, E. A. Zhukov, V. N. Filatov, and N. Y. Sorokin, J. Magn. Magn. Mater. **238**, 109 (2002).
[27] A.P. Kuzmenko, E. A. Zhukov, and Y. I. Shcherbakov, Tech. Phys. **53**, 1433 (2008).
[28] A. M. Kalashnikova, A. V. Kimel, R. V. Pisarev, V. N. Gridnev, A. Kirilyuk, and Th. Rasing, Phys. Rev. Lett. **99**, 167205 (2007).
[29] D. L. Dorofeev, G. V. Pakhomov, and B. A. Zon, Phys. Rev. E **71**, 026607 (2005).
[30] Z.-G. Ye, B. Noheda, M. Dong, D. Cox, and G. Shirane, Phys. Rev. B **64**, 184114 (2001).
[31] J.-M. Kiat, Y. Uesu, B. Dkhil, M. Matsuda, C. Malibert, and G. Calvarin, Phys. Rev. B **65**, 064106 (2002).
[32] K. Y. Chan, W. S. Tsang, C. L. Mak, K. H. Wong, and P. M. Hui, Phys. Rev. B **69**, 144111 (2004).
[33] G. T. Rado, R. W. Wright, and W. H. Emerson, Phys. Rev. **80**, 273 (1950).
[34] G. T Rado, Phys. Rev. **83**, 821 (1951).
[35] G. B. Scott, J. Phys. D: Appl. Phys. **7**, 1574 (1974).
[36] Y. S. Didosyan, H. Hauser, and F. Haberl, Sensors and Actuators A **92**, 67 (2001).
[37] V. G. Bae'yakhtar, B. A. Ivanov, and M. V. Chetkin, Sov. Phys. Usp. **28**, 563 (1985).
[38] N. S. Tzannes, IEEE Trans. Sonics and Ultrasonics **13**, 33 (1966).
[39] A. M. Kadomtseva, A. P. Agafonov, V. N. Milov, A. S. Moskvin, and S. A. Semenov, Fizika Tverdogo Tela **23**, 3554 (1981).
[40] A. P. Kuzmenko, E. A. Zhukov, V. N. Filatov, and M. B. Dobromyslov, J. Magn. Magn. Mater. **257**, 327 (2003).
[41] Y. S. Didosyan, H. Hauser, and G. A. Reider, IEEE Tran. Magn. **38**, 3243 (2002).
[42] R. Zhang, B. Jiang, and W. Cao, J. Appl. Phys. **90**, 3471 (2001).